Role of electron saddle swaps in the photon spectra following Li^{3+} charge-exchange collisions with $H^*(n = 2)$, $Na(3s)$, $Na^*(3p)$, and $Li(2s)$ targets

S. Otranto,[1,*] R. Hoekstra,[2] and R. E. Olson[3]

[1]*IFISUR and Departamento de Física, Universidad Nacional del Sur, 8000 Bahía Blanca, Argentina*

[2]*Zernike Institute for Advanced Materials, University of Groningen, NL 9747 AG, Groningen, The Netherlands*

[3]*Department of Physics, Missouri University of Science and Technology, Rolla Missouri 65409, USA*

(Received 15 January 2014; published 14 February 2014)

The role of electron saddle swaps in collisions of bare Li with metastable hydrogen and alkali-metal atoms is investigated by means of the classical trajectory Monte Carlo method. In particular, we show that oscillations as a function of collision energy in the photon spectra resulting from charge exchange are directly related to the number of potential-saddle crossings that a receding electron can achieve during a given reaction. The range of impact energies spanned is 0.01–50 keV/amu, an area of interest for diagnostic purposes in tokamak nuclear fusion power reactors.

DOI: 10.1103/PhysRevA.89.022705 PACS number(s): 34.70.+e

I. INTRODUCTION

Charge-exchange spectroscopy is a powerful diagnostic tool that is applied to tokamak plasmas. From the photonic emission that follows the charge-exchange collisions, information on the plasma temperature, its rotation, and the amount of impurities present inside the reactor can be gained [1,2]. The fiber optics between the thermonuclear reactor vessel and the spectrometers restrict the charge-exchange spectroscopy observations to the visible range (1.771–3.1 eV). Charge-exchange reactions between deuterium (the dominant component of the plasma) and impurities such as Ne^{10+}, C^{6+}, and Li^{3+} provide photons in the visible range arising from $12 \rightarrow 11$ and $11 \rightarrow 10$, $8 \rightarrow 7$, and $5 \rightarrow 4$ transitions, respectively. However, for these ions the n shells dominantly populated follow the $n_{\max} = \sqrt{V_{\rm ion}/13.6}\, q^{3/4}$ scaling law [3] and are explicitly given by $n_{\max} = 6, 4$, and 2, respectively. The notation $V_{\rm ion}$ refers to the ionization potential of the target atom in units of eV. As a result, only a minor signal in the visible range is expected to arise from reactions with ground-state D [2].

On the other hand, at low impact energies even a very tiny fraction of metastable deuterium [$D^*(n = 2)$, $V_{\rm ion} = 3.4$ eV] present in the plasma, which is usually in the range of 0.1%–1%, may fully dominate the visible range emission [2]. This is because capture cross sections to high-lying states are enhanced by several orders of magnitude compared to those from the ground state [$n_{\max} = 11$, 8, and 5 for +10, +6, and +3 projectiles with $D^*(n = 2)$], and provide a strong signal for diagnostics. In this sense, reliable charge-exchange cross sections are needed for bare projectiles impinging on $D^*(n = 2)$ in order to calculate effective emission coefficients for these H-like spectral lines [4]. Hereafter, we will refer to $H^*(n = 2)$ instead of $D^*(n = 2)$ since their cross sections are equivalent at the same collision velocity or keV/amu.

Since $H^*(n = 2)$ is not a feasible target for laboratory experiments, in recent years magneto-optical-trap-recoil-ion momentum-spectroscopy experiments have been conducted at KVI-Groningen using different alkali-metal targets, $Li(2s)$, $Na(3s)$, and $Na^*(3p)$, since their ionization potentials are similar to $H^*(n = 2)$ [5–7]. It is expected that charge-exchange information on $H^*(n = 2)$, which has $V_{\rm ion} = 3.4$ eV, can be interpolated from the results obtained for $Na(3s)$ ($V_{\rm ion} = 5.14$ eV) and $Na^*(3p)$ ($V_{\rm ion} = 3.04$ eV).

In a recent joint collaboration with the Groningen group, we have studied state-selective charge-exchange processes between He-like projectiles (in particular, N^{5+} and Ne^{8+}) with $Na(3s)$ and $Na^*(3p)$. Their angular differential studies evidenced an energy-dependent oscillatory structure which was well reproduced by classical trajectory Monte Carlo (CTMC) calculations and was ascribed to the possible different numbers of electron saddle crossings which take place during the capture process [7,8]. Early on, oscillations were observed on the visible line emission cross sections for C^{6+} and O^{8+} collisions on $Li(2s)$ but their origin due to electron swaps went unrecognized [9].

The electron saddle swap mechanism was first invoked to describe oscillations on the total cross sections for ion–Rydberg atom charge-exchange collisions [10]. Interestingly, the classical description of the active electron swapping centers during the collision provides an alternative view to the stationary phase argument recalled in quantal or semiclassical studies [11–13]. Following this line, Schultz *et al.* elaborated on the electron swap thesis and showed that the oscillatory total cross section for He^{2+}+H excitation was also due to electron swaps [14]. A quantal description of this particular reaction based on the phase interference of two paths beginning from the initial state leading to a common final state was soon after given by Krstic *et al.* [15].

In this work, we extend our theoretical investigation to the charge-exchange processes occurring in Li^{3+} collisions with $H^*(n = 2)$, $Li(2s)$, $Na(3s)$, and $Na^*(3p)$ at impact energies in the range 0.01–50 keV/amu which are of direct relevance for tokamak devices. Moreover, since in very many of the fusion plasma applications the populations of lm states within a specific n-shell get redistributed due to collisions or electric fields, we present the n-shell cross sections only along with some specific field-free line emission cross sections. Line emission cross sections for the $5 \rightarrow 4$ transition (visible range), Lyman lines, and x-ray hardness ratios R for these collision systems are shown because of their importance in determining the energy balance in tokamak reactor divertors.

*Corresponding author: sotranto@uns.edu.ar

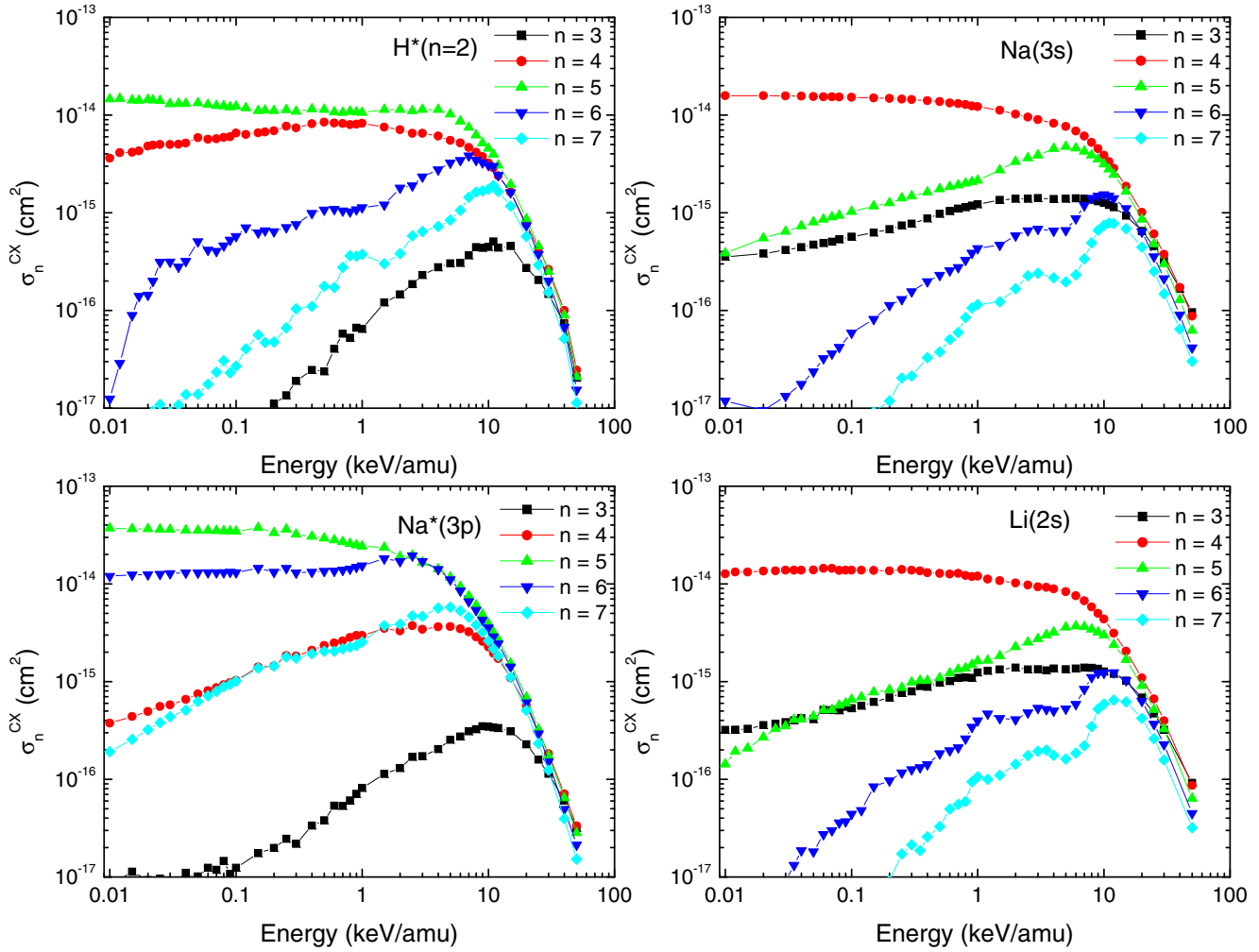

FIG. 1. (Color online) CTMC state-selective charge-exchange cross sections for Li^{3+} collisions on $H^*(n=2)$, Na($3s$), $Na^*(3p)$, and Li($2s$), as a function of the projectile impact energy.

What is quite surprising is the paucity of photon emission data for the above collision systems. Data only exit for B^{3+} partially stripped ions colliding with Na($3s$). This data are presented and used to benchmark our calculations.

II. THEORETICAL METHOD

The CTMC calculations rely on the numerical evaluation of a mutually interacting three-body system. For the Na^+ (or Li^+) core interaction with the electron and the projectile, we have used the central model potential of Garvey *et al.* [16] where the effective charge seen by the active electron and the projectile depends on their radial distances with respect to the target core. For each capture event, a classical number n_c is obtained from the binding energy E_p of the electron relative to the projectile by

$$E_p = -q^2/(2n_c^2), \tag{1}$$

where q is the charge of the projectile core. Then, n_c is related to the quantum number n of the final state by the Becker and McKellar binning rule [17],

$$[(n-1)(n-1/2)n]^{1/3} \leqslant n_c \leqslant [n(n+1)(n+1/2)]^{1/3}. \tag{2}$$

From the normalized classical angular momentum $\boldsymbol{l}_c = (n/n_c)(\boldsymbol{r}\times\boldsymbol{k})$, where $\mathbf{r}$ and $\mathbf{k}$ are the captured electron position and momentum relative to the projectile, we relate l_c to the orbital quantum number l of the final state by

$$l \leqslant l_c \leqslant l+1. \tag{3}$$

The cross section to a definite nl state is then given by

$$\sigma_{nl} = N(n,l)\pi b_{\max}^2/N_{\text{tot}}, \tag{4}$$

where $N(n,l)$ is the number of events of electron capture to the nl level and N_{tot} is the total number of trajectories integrated. The impact parameter $b_{\max}$ is the parameter beyond which the probability of electron capture is negligibly small.

For each trajectory, an electron swap is recorded each time the electron position vector component along the internuclear axis ($\mathbf{r}_e\cdot\mathbf{R}$) crosses the potential-saddle position r_{saddle} as a function of the internuclear distance R. For the present Garvey representation of the target, the position of the saddle can be parametrized as $r_{\text{saddle}} = r_{COB} + aR^2e^{-\lambda R} + bR^2e^{-\gamma R}$, with $r_{COB} = R/(\sqrt{Z_p}+1)$ (the saddle position predicted by the classical overbarrier model for the hydrogen target [18]). As noted in [8], we observe that compared to the hydrogenic model the Garvey parametrization shifts the potential saddle

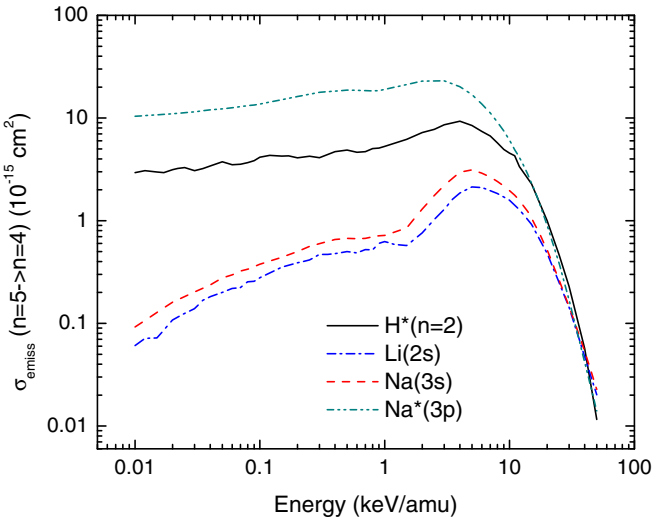

FIG. 2. (Color online) Line emission cross section for the $5 \rightarrow 4$ transition following charge exchange in Li^{3+} collisions with $H^*(n = 2)$, $Na(3s)$, $Na^*(3p)$, and $Li(2s)$.

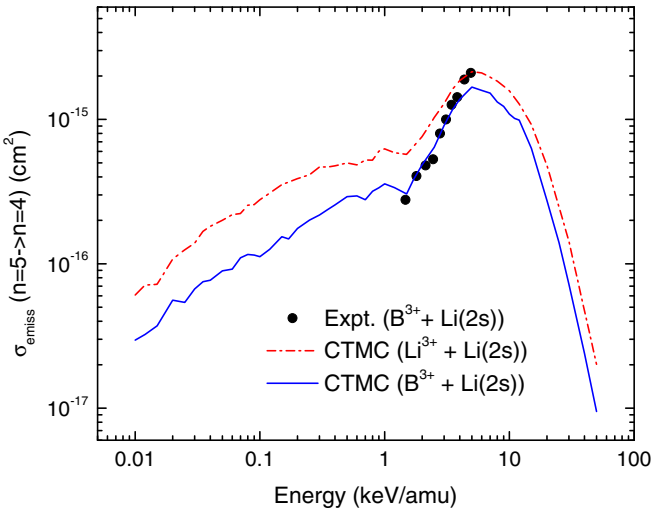

FIG. 3. (Color online) Line emission cross section for the $5 \rightarrow 4$ transition following charge exchange in B^{3+} collisions with $Li(2s)$.

to larger distances for low R values. This clearly indicates that for the present case the target ion's area of influence extends to larger distances than predicted by the standard overbarrier model [18]. Additionally, as the impact energy is lowered, the electron can move in the field generated by both ions for longer periods of time, and the possible number of swaps leading to electron capture increases.

III. RESULTS

A. Charge exchange

First, we consider the n-state selective cross sections for 0.01–50 keV/amu Li^{3+} collisions on $H^*(n = 2)$, $Na(3s)$, $Na^*(3p)$, and $Li(2s)$ (Fig. 1). Electron capture at low impact energies populates one or two specific energy levels (5 and 6, 4, 3 and 4, and 4, respectively) according to their V_{ion} values. At larger impact energies the n distributions widen and more final states turn available from the charge-exchange process.

The principal n level for capture is 5 for $H^*(n = 2)$ and $Na^*(3p)$ and 4 for $Na(3s)$ and $Li(2s)$. This is related to their respective V_{ion} values. In all cases, oscillatory structures appear for n values greater than the principal n level for capture.

Because of the relevance the present collision systems can have for tokamak diagnostics, in Fig. 2 we show explicitly the line emission cross section for the $5 \rightarrow 4$ transition in the visible spectral range as a function of impact energy for all the targets considered. It can be seen that the line emission cross sections for collisions on $H^*(n = 2)$ are bracketed by those of the $Na(3s)$ and $Na^*(3p)$ targets. At impact energies below about 5 keV/amu the $Na^*(3p)$ cross sections show an energy dependence similar to the $H^*(n = 2)$ results despite the fact that they are larger by a factor of about 3.3. At impact energies larger than 20 keV/amu, the $Na^*(3p)$ results are almost the same as the $H^*(n = 2)$ ones.

Since no experimental data are available to test our predictions, in Fig. 3 we contrast our line emission cross sections to experimental data taken at KVI University of Groningen for B^{3+}+$Li(2s)$ collisions in the energy range 1.5–5 keV/amu. The data were obtained during a whole series of measurements on low-Z ions interacting with Li [19,20], but never released. Experimental details and procedures can be found in Refs. [19,20]. The systematic absolute uncertainty in the data is some 20% mainly due to the normalization to proton data. Statistical uncertainties increase from 10% to 20% when going from the highest (5 keV/amu) to the lowest (1.5 keV/amu) energy used. We also add the CTMC line emission cross sections for the bare Li projectile as well, to visually display the differences arising from the filled K shell of the projectile. While for Li^{3+} projectiles cascade contributions from higher n shells have been accounted for by using the hydrogenic transition rates [21], for B^{3+} projectiles we have used the transition rates tabulated by Fuhr and Wiese [22]. There is very good agreement between the experimental data and the CTMC predictions except at the highest energies.

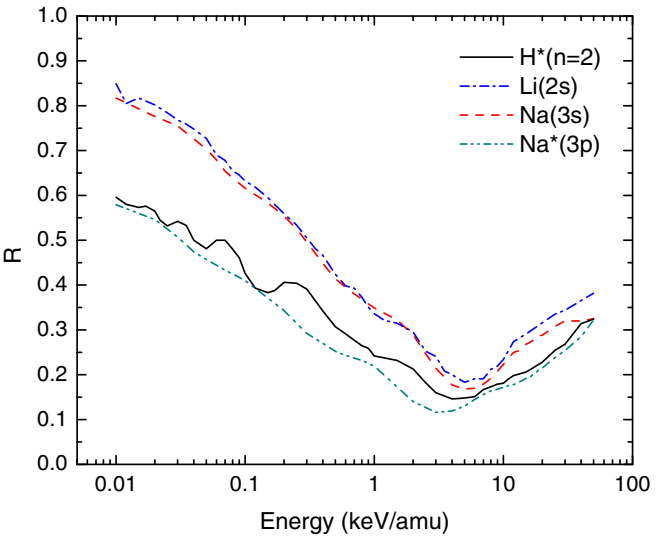

FIG. 4. (Color online) Hardness ratio as a function of impact energy for Li^{3+} collisions with $H^*(n = 2)$, $Na(3s)$, $Na^*(3p)$, and $Li(2s)$.

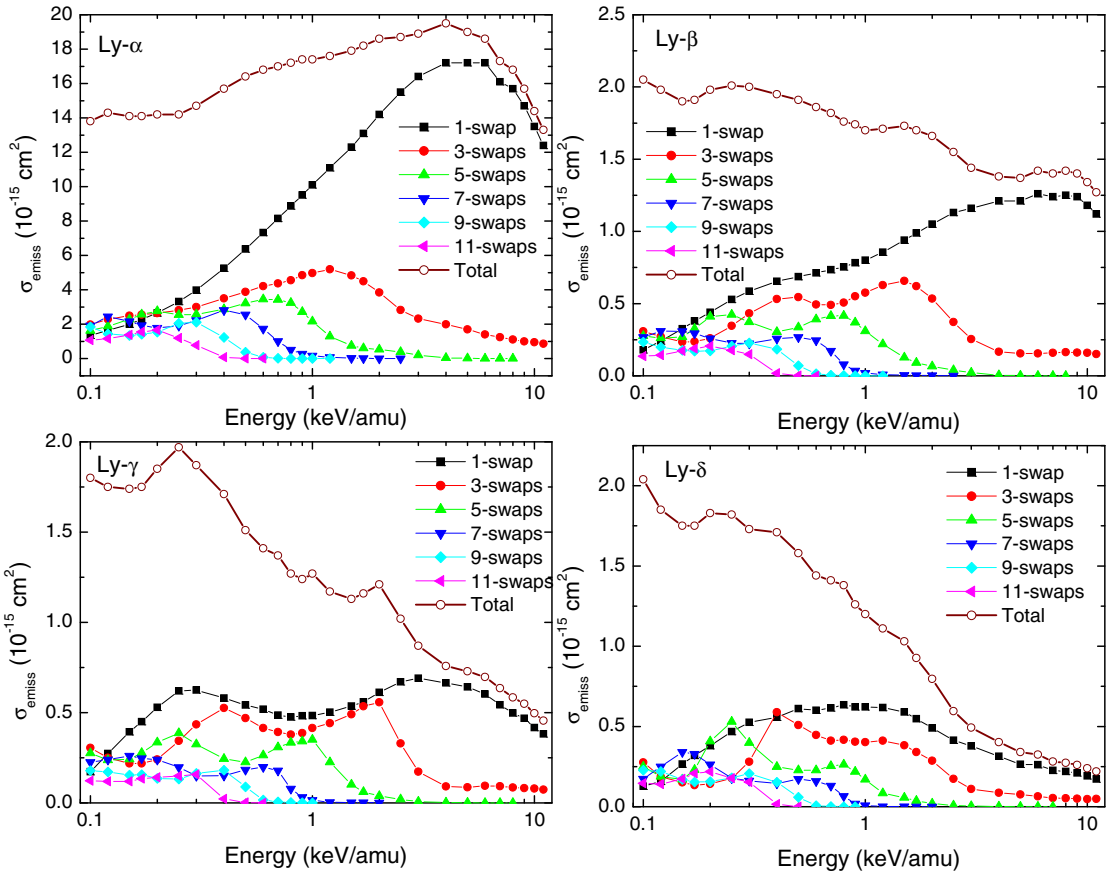

FIG. 5. (Color online) Line emission cross sections corresponding to the first four Lyman lines in Li^{3+} collisions with $H^*(n = 2)$.

A more detailed inspection of the line emission cross sections can be made via the exploration of the Lyman lines ($np \rightarrow 1s$ transitions). A useful way to highlight whether capture takes place to low or large l values is by means of the hardness ratio (R) which provides the ratio of the intensity arising from the higher Lyman lines ($np \rightarrow 1s$ transitions with $n \geq 3$) to the Lyman-α line ($2p \rightarrow 1s$).

In Fig. 4, we show the hardness ratio R as a function of the impact energy for the targets under consideration. All targets exhibit a minimum in the hardness ratio localized in the 3–7 keV/amu range. The $H^*(n = 2)$ results are again more similar to the $Na^*(3p)$ calculations than to those obtained for $Li(2s)$ and $Na(3s)$. Moreover, despite that all targets exhibit a somewhat oscillatory structure for their hardness ratios, we note that the one corresponding to $H^*(n = 2)$ is most pronounced. To gain insight into the origin of these oscillations, in Fig. 5 we show the swaps contributions to the Ly-α, Ly-β, Ly-γ, and Ly-δ lines. It can then be seen that as the impact energy is lowered, more swaps can make a significant contribution and leave a clear trace in the line emission cross section. The oscillations obtained for the R value are due to the joint contribution of these individual structures.

Another view is provided by the l distributions. Provided that for these targets the principal capture levels at keV/amu energies are given by $n = 4$ and 5, in Fig. 6 we show the $4l$- and $5l$-state selective cross sections for Li^{3+} collisions with $H^*(n = 2)$. These cross sections also evidence oscillatory structures as a function of impact energy which, based on

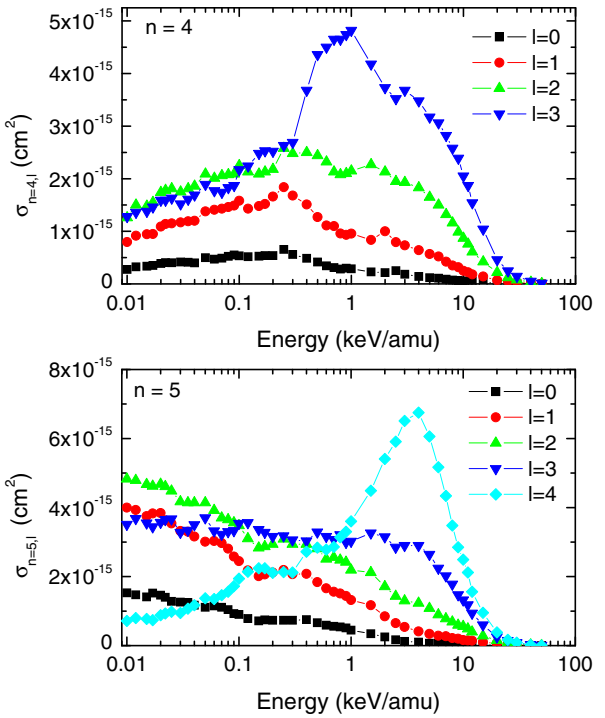

FIG. 6. (Color online) CTMC l-state selective charge-exchange cross sections for $n = 4$ and 5 as a function of the impact energy in Li^{3+} collisions with $H^*(n = 2)$.

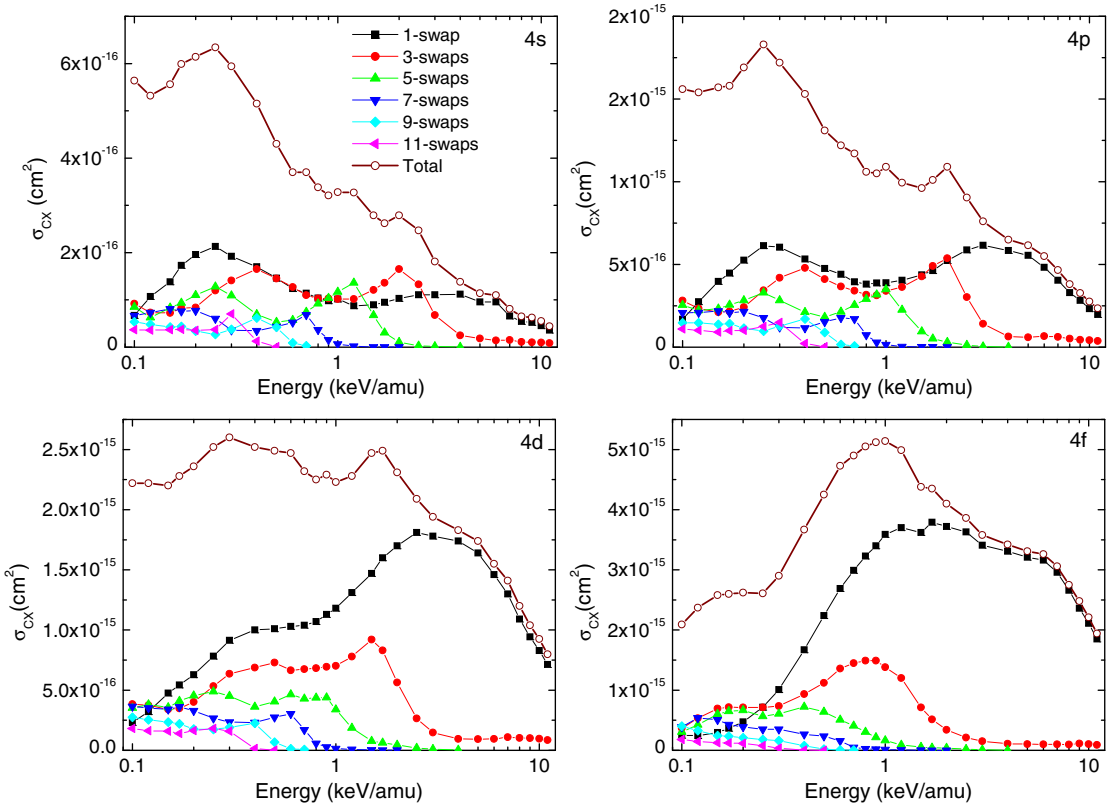

FIG. 7. (Color online) CTMC l-state selective charge-exchange cross sections for $n = 4$ as a function of the impact energy in Li^{3+} collisions with $H^*(n = 2)$. The contributions of the different swaps are explicitly shown.

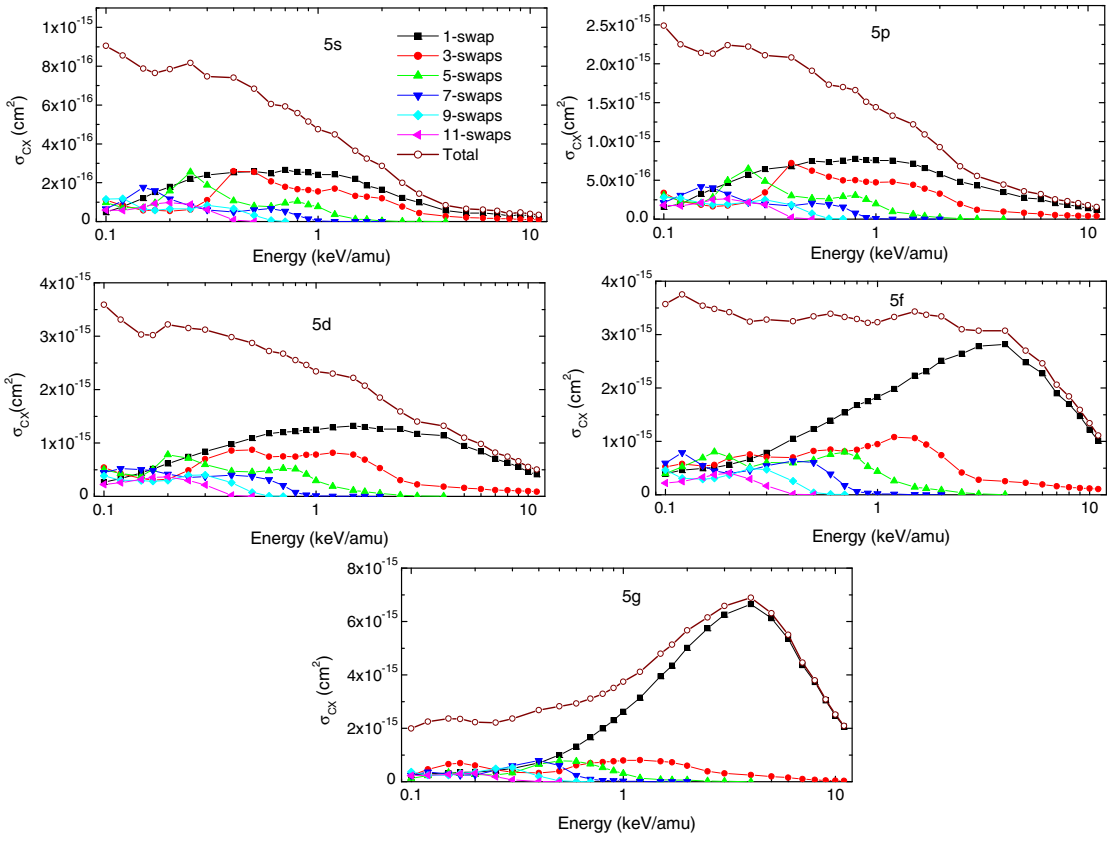

FIG. 8. (Color online) CTMC l-state selective charge-exchange cross sections for $n = 5$ as a function of the impact energy in Li^{3+} collisions with $H^*(n = 2)$. The contributions of the different swaps are explicitly shown.

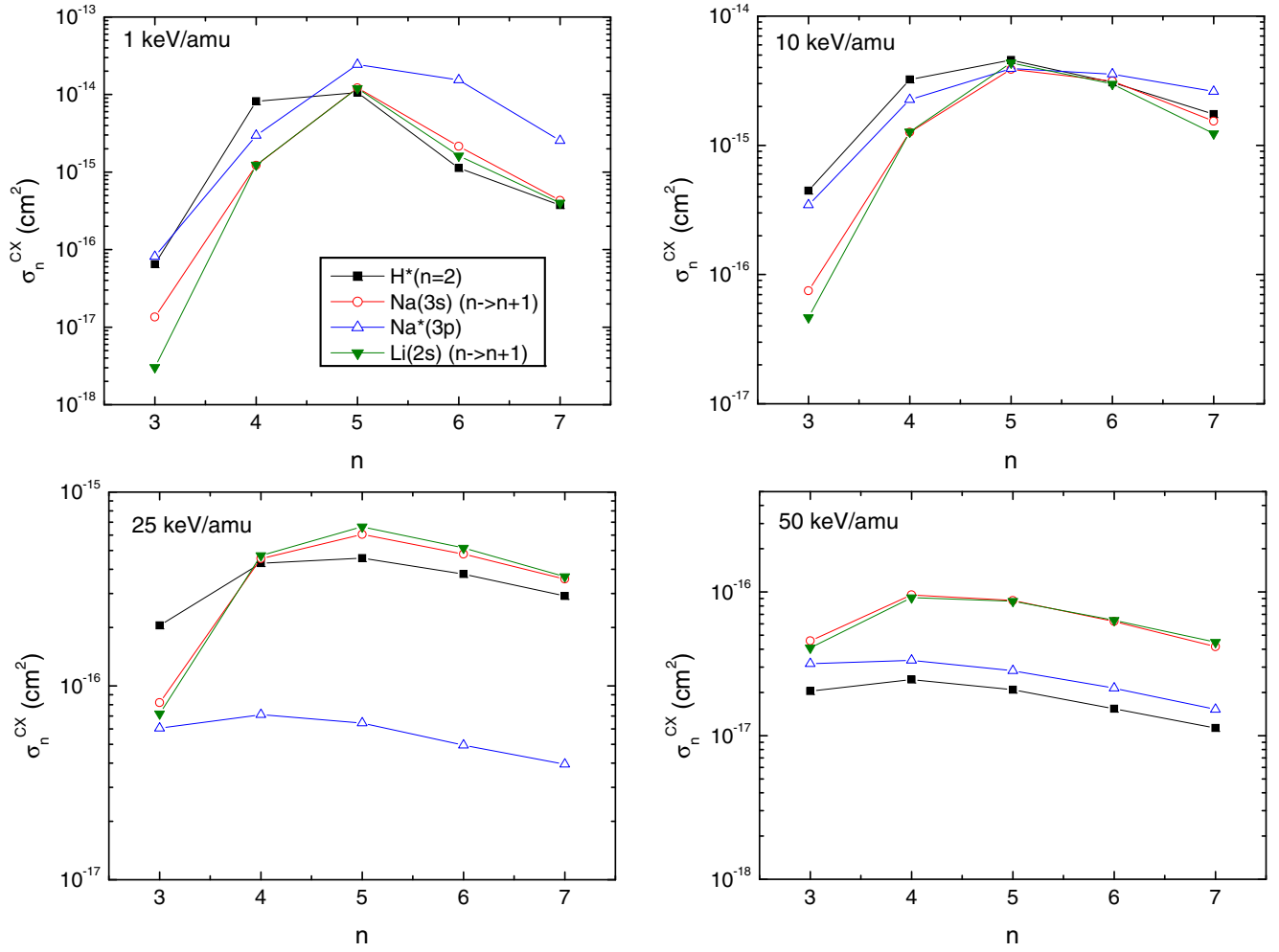

FIG. 9. (Color online) CTMC charge-exchange n distributions for Li^{3+} collisions on $H^*(n=2)$, Na($3s$) (shifted up by one n level), $Na^*(3p)$, and Li($2s$) (shifted up by one n level) at impact energies 1, 10, 25, and 50 keV/amu.

our previous comments, one would naturally relate to the contributions from different swaps. To confirm our hypothesis, in Figs. 7 and 8 we present the swaps contributions to the l distributions as a function of impact energy for $n = 4$ and 5.

It can be seen that at impact energies on the order of 10 keV/amu, charge exchange takes place via a single swap. On the other hand, as the impact energy is lowered, more swaps become relevant and at an impact energy of 0.1 keV/amu, up to 11 swaps need to be considered to reach convergence.

Now, coming back to the use of studying alkali-metal targets as potential substitutes for $H^*(n = 2)$, in Ref. [6] a scaling was proposed based on the theoretical and experimental data obtained from Ne^{8+}+Na($3s$) collisions in the keV/amu energy range to provide a first-order estimate for $H^*(n = 2)$. This scaling was based on CTMC calculations and consisted in shifting the n distributions corresponding to Na($3s$) up by one n level together with an overall magnitude scaling factor of 1.3. These studies complement previous theoretical scalings introduced by Cornelius *et al.* [23] for the state-selective charge-exchange cross sections between bare ions of charge q and $H^*(n = 2)$, Li($2s$), and $Li^*(2p)$ targets. In Fig. 9, we perform an inspection of the n distributions at impact energies of 1, 10, 25, and 50 keV/amu for $H^*(n = 2)$, Na($3s$), and $Na^*(3p)$ targets. In all cases, the n distributions corresponding to Na($3s$) were shifted up by one n level according to our previous experience with Ne^{8+} projectiles. However, we have not included any overall scaling factor, in order to properly infer the physical trends exhibited by the different collision systems at the impact energies explored.

At 1 keV/amu, and despite the fact that the principal capture number predicted for the three collision systems is $n = 5$, the profile of the n distribution obtained for $H^*(n = 2)$ cannot be properly reproduced either by the shifted Na($3s$) distribution nor the $Na^*(3p)$ distribution. This is in contrast with our former results for Ne^{8+} projectiles where very close agreement was observed between the $H^*(n = 2)$ and the scaled Na($3s$) distributions. The n distributions covering the 1–10 keV/amu range provide evidence that the $H^*(n = 2)$ distributions are in better agreement with the $Na^*(3p)$ distributions for n values lower than the principal capture level, while they are in better agreement with the shifted Na($3s$) distributions for n values larger than the principal capture level. As the impact energy

increases (25 keV/amu) the distributions flatten, with many more n-levels gaining relevance from charge exchange, and the cross sections' magnitudes corresponding to Na($3s$) dominate over those corresponding to Na*($3p$). Finally, as we move up to 50 keV/amu, the Na*($3p$) results provide the closest agreement with H*($n = 2$).

IV. CONCLUSIONS

In this article we have studied the role of the electron saddle swaps in charge-exchange processes between Li^{3+} ions and H*($n = 2$), Na($3s$), Na*($3p$), and Li($2s$) targets. These systems are of particular interest for charge-exchange spectroscopy of tokamak plasmas. Oscillatory structures have been found in the line emission cross sections which also leave an oscillatory trace in the x-ray hardness ratio parameter. We have shown that these structures are related to the possible number of potential-saddle swaps the captured electron can undergo during the capture process.

We have also explored whether the present results for the alkali-metal, tractable targets from an experimental point of view, would provide a fast route to gain insight into H*($n = 2$). From the present results, we conclude that an ultimate scaling of the H*($n = 2$) cross sections based on theoretical and experimental cross sections for alkali-metal targets is not yet at hand and more effort is needed in this direction.

ACKNOWLEDGMENTS

Work at Universidad Nacional del Sur is supported by Grants No. PGI 24/F059 and No. PIP 112-201101-00749 of CONICET (Argentina).

[1] R. C. Isler, Plasma Phys. Controlled Fusion **36**, 171 (1994).
[2] R. Hoekstra, H. Anderson, F. W. Bliek, M. Von Hellermann, C. F. Maggi, R. E. Olson, and H. P. Summers, Plasma Phys. Controlled Fusion **40**, 1541 (1998).
[3] R. E. Olson, Phys. Rev. A **24**, 1726 (1981).
[4] H. Anderson, M. G. von Hellermann, R. Hoekstra, L. D. Horton, A. C. Howman, R. W. T. Konig, R. Martin, R. E. Olson, and H. P. Summers, Plasma Phys. Controlled Fusion **42**, 781 (2000).
[5] V. G. Hasan, S. Knoop, R. Morgenstern, and R. Hoekstra, J. Phys.: Conf. Ser. **58**, 199 (2007).
[6] I. Blank, S. Otranto, C. Meinema, R. E. Olson, and R. Hoekstra, Phys. Rev. A **85**, 022712 (2012).
[7] I. Blank, S. Otranto, C. Meinema, R. E. Olson, and R. Hoekstra, Phys. Rev. A **87**, 032712 (2013).
[8] S. Otranto, I. Blank, R. E. Olson, and R. Hoekstra, J. Phys. B: At. Mol. Opt. Phys. **45**, 175201 (2012).
[9] R. E. Olson, J. Pascale, and R. Hoekstra, J. Phys. B: At. Mol. Opt. Phys. **25**, 4241 (1992).
[10] K. B. MacAdam, J. C. Day, J. C. Aguilar, D. M. Homan, A. D. MacKellar, and M. J. Cavagnero, Phys. Rev. Lett. **75**, 1723 (1995).
[11] R. B. Bernstein, in *Molecular Beams*, edited by J. Ross (Interscience Publishers, New York, 1966), Chap. 3, pp. 75–134.
[12] J. Perel, R. H. Vernon, and H. L. Daley, Phys. Rev. **138**, A937 (1965).
[13] R. E. Olson, Phys. Rev. **187**, 153 (1969).
[14] D. R. Schultz, C. O. Reinhold, and P. S. Krstic, Phys. Rev. Lett. **78**, 2720 (1997).
[15] P. S. Krstic, C. O. Reinhold, and D. R. Schultz, J. Phys. B: At. Mol. Opt. Phys. **31**, L155 (1998).
[16] R. H. Garvey, C. H. Jackman, and A. E. S. Green, Phys. Rev. A **12**, 1144 (1975).
[17] R. L. Becker and A. D. McKellar, J. Phys. B: At. Mol. Opt. Phys. **17**, 3923 (1984).
[18] A. Niehaus, J. Phys. B: At. Mol. Opt. Phys. **19**, 2925 (1986).
[19] R. Hoekstra, E. Wolfrum, J. P. M. Beijers, F. J. de Heer, H. Winter, and R. Morgenstern, J. Phys. B: At. Mol. Opt. Phys. **25**, 2587 (1992).
[20] R. Hoekstra, R. E. Olson, H. O. Folkerts, E. Wolfrum, J. Pascale, F. J. de Heer, R. Morgenstern, and H. Winter, J. Phys. B: At. Mol. Opt. Phys. **26**, 2029 (1993).
[21] H. A. Bethe and E. E. Salpeter, *Quantum Mechanics of One and Two-Electron Atoms* (Springer, Berlin, 1957).
[22] J. R. Fuhr and W. L. Wiese, J. Phys. Chem. Ref. Data **39**, 013101 (2010).
[23] K. R. Cornelius, K. Wojtkowski, and R. E. Olson, J. Phys. B: At. Mol. Opt. Phys. **33**, 2017 (2000).